The role played by viscoelasticity in the bulk material during the propagation of a dynamic crack in elastomers

Vasudevan Kamasamudram, Michel Coret, Nicolas Moës

The role played by viscoelasticity in the bulk material during the propagation of a dynamic crack in elastomers

Vasudevan Kamasamudram · Michel Coret · Nicolas Moës

Abstract Investigation of dynamic fracture of elastomers can still be considered to be a relatively open area. When a sheet of elastomer is stretched in a tensile machine and a crack is introduced, the crack propagates at a speed that depends on the initial stretch level. There are instances where this speed is noted to exceed the shear wave speed based on the elastic modulus under high imposed stretches. Such cracks are called transonic cracks. It was usually hypothesized that either the hyperelastic or viscoelastic stiffening of the bulk material raises the wave speeds resulting in crack speeds entering the transonic regime. This article revisits the experiments performed on Polyurethane elastomers in Corre et al. (Int J Fract 224(1):83–100, 2020) to study the implications of both these hypotheses. Crack propagation has not been explicitly modeled, but the crack speeds are implicitly imposed on the geometry using the boundary conditions extracted from the experimental data. It has been determined that the viscoelasticity in the bulk is needed to describe and understand the transonic cracks in polyurethane elastomer. The inclusion of viscoelasticity results in the notions of 'rubbery' and 'glassy' wave speeds and hence, the transonic regime is defined considering the rubbery wave speed.

Keywords Dynamic fracture · Viscoelasticity · Transonic cracks · Elastomer

V. Kamasamudram (✉) · M. Coret · N. Moës
GeM Institute, UMR CNRS 6183, Centrale Nantes, 1 rue de la Noë, Nantes 44321, France
e-mail: vasudevan.kamasamudram@ec-nantes.fr

M. Coret
e-mail: michel.coret@ec-nantes.fr

N. Moës
e-mail: nicolas.moes@ec-nantes.fr

N. Moës
Institut Universitaire de France, Paris, France

1 Introduction

Theoretically, a crack propagating in a solid can travel as fast as a Rayleigh wave, c_R (Freund 1990), although in reality, such a speed is hardly achieved. Cracks are known to branch at speeds of about 40% to 60% of c_R (Ravi-Chandar and Knauss 1984; Sharon et al. 1996). Often special techniques such as introducing a weak plane or weakening the material in the prospective crack path are needed to prevent or at least delay the branching event and make the crack propagate at about 90% of c_R (Washabaugh and Knauss 1994). However, in some instances, cracks propagating along weak planes under mode-II loading were observed to travel faster than the shear wave and such cracks are called Transonic cracks. The theory of LEFM has been extended to include such cracks (Freund 1979, 1990; Huang and Gao 2001). For mode-II cracks in this regime, a Mach cone corresponding to shear wave along which the particle speeds exhibit discontinuities have been experimentally observed to tail the crack tip (Rosakis et al. 2000; Rosakis 2002). The existence of

these cracks have been confirmed numerically (Needleman 1999) as well.

Some studies, such as in Petersan et al. (2004), Chen et al. (2011), Marder (2006), performed on elastomers reveal that the cracks can travel at speeds that exceed the speed of elastic shear wave, c_s, when subjected to high stretch ratios. Recent experiments by Corre et al. (2020), Morishita et al. (2016) also confirm this observation. As a reminder, Linear Elastic Fracture Mechanics (LEFM) forbids the crack speed from exceeding c_R (Freund 1990) for a Mode-I crack. Earlier experimental works on the fracture of elastomer membranes, for instance, Gent and Marteny (1982) and balloons (Stevenson and Thomas 1979) also report 'higher' crack speeds when compared to the wave speeds. They attribute this to an increase in the stiffness of the material (and hence the wave speeds) in the vicinity of the crack tip because of either the higher strain rates and viscoelastic effects or the higher strains at the tip and hyperelastic stiffening. However, these articles make no specific mention about Transonic cracks.

Some analytical (Guo et al. 2003) and numerical (Buehler et al. 2003) works investigate the effect of local hyperelastic stiffening on the crack speeds. In Buehler et al. (2003), a material that increases its stiffness (by a factor of 4) after a certain strain level (called onset strain) has been used to investigate crack speeds obtained. Molecular dynamics simulation was used for this purpose and the crack path is constrained to the center of the specimen to prevent branching. It was observed that the crack speed entered the Transonic regime starting from a certain value of the onset strain. It has been mentioned, however, that in such a case, 'Mach cones of shear wave front' were observed. In Guo et al. (2003), a steady state crack motion has been investigated in a material with an upturn in stress strain curve in mode-III. In the vicinity of the crack tip where the strains are higher (because of presence of the crack tip and hence strain concentration), the modulus is higher and so are the wave speeds. The equations of motion, hence, when written in this region, maintain their ellipticity. However, in the region farthest from the tip where the strains are smaller, the modulus and hence the wave speeds are smaller than the crack speed and hence the equations of motion become hyperbolic. A discontinuity in stresses along the boundary separating these two regions can be noted along with discontinuities in the region where the material has a smaller modulus.

Some lattice based models have been used in Chen et al. (2011), Marder (2006) where Transonic cracks were observed in elastomers. In those references, a shock wave theory for fracture has been proposed as well. However, Chen et al. (2011), Marder (2006) do not report a shock wave that tails the crack tip in either their simulations or the experiments. They instead treat the crack faces behind the tip to be of a wedge shape (noted to be 'strikingly similar to Mach cone' in Petersan et al. (2004)) in the Transonic regime. This is different from the shock front in the usual sense where the first time and spatial derivatives of displacement exhibit discontinuity along a moving surface. From the experiments performed on specimens of different geometries, Chen et al. (2011) concluded that the crack speed depends only on the applied stretch and not on the specimen geometry once the crack goes into the Transonic regime, while it is seen to depend on specimen geometry as well in the subsonic regime.

In this article, the experiments performed by Corre et al. (2020) will be examined further to check for the presence of discontinuities in velocity and strain in the transonic regime. Such fronts have been observed in the impact and retraction tests performed on latex rubber and SBR in Niemczura and Ravi-Chandar (2011a, b), although their existence does not match the theoretical predictions using a Hyperelastic model based on the theory in Knowles (2002). This discrepancy has been attributed to the hysteretic behavior of the material.

It will be determined if hyperelastic stiffening of the bulk material mentioned in the earlier studies is necessary (and sufficient) to reproduce the displacement and velocity fields observed in the experiments for cracks propagating in sub- and trans-sonic regimes. The effect of viscoelasticity in the bulk will be examined as well. The propagation of crack will not be explicitly modeled. Instead, the crack speeds will be implicitly imposed onto the geometry using the methodology described in Sect. 3. Explicit modeling of crack and rate effects at the crack tip will be presented in another article. The FE software ABAQUS (Abaqus 2014) will be used. Section 2 will present the results and additional observations of the experiments performed in Corre et al. (2020). Section 3 contains the methodology used and some numerical analysis performed using various constitutive models and the resulting observations. Sections 4 and 5 contain further discussions and conclusions.

2 Experimental analysis

In Corre et al. (2020), a Polyurethane specimen is stretched to a required strain level in a pure shear configuration and a seed crack is then introduced at one end. In this section, the velocity and strain fields from those tests will be analyzed further.

To be self-sufficient, a brief summary of the test protocol followed in the mentioned reference will be included below.

2.1 Test protocol and data acquisition

Experiments were conducted on 200 mm long (taken as x-direction), 40 mm tall (y-direction) and 3 mm thick (z-direction) specimens in Corre et al. (2020). The test protocol is as below.

- The specimen is held along the longest side between the jaws of a tensile machine using the supports molded onto its top and bottom.
- Once secured, the specimen is stretched by pulling the top jaw of the Instron machine at a speed of 20 mm min^{-1}.
- Once the target stretch level ($\lambda = \frac{h_f}{h_0}$, h_f is the final specimen height and h_0 is the initial height—40 mm) is reached, a crack of about 3 to 4 mm long is introduced at the left end of the specimen in the middle using a razor blade.

The crack then propagates through the specimen, breaking it into two pieces. A High Resolution (HR) and a High Speed (HS) camera are used to monitor the whole experiment. The HR camera captures the images at a rate of about 3 fps, while the HS camera captures at rates between 10,000 and 30,000 fps. The HR camera is hence used to record the initial stretching of the specimen while the HS camera records the fracture process. The HS camera is managed by a device that stops the camera once the crack breaks the specimen. The propagation of crack leads to a drop in the reaction forces on the Instron machine which the triggering device keeps a track of to stop the HS camera. The data from both the cameras are then used to obtain the displacement fields in the specimen during the entire experiment using the DIC technique using VIC-2D software (VIC-2D CS 2009). The images recorded during the initial stretch and the crack propagation steps can be found at Coret and Corre (2017).

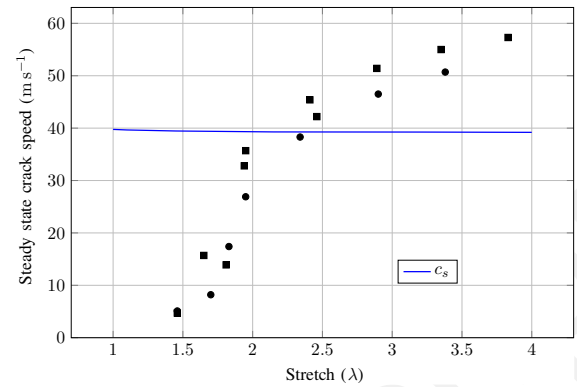

Fig. 1 Experimental results for 40 mm tall samples from Corre et al. (2020)

2.2 Additional observations on the 40 mm specimen

The distinction of crack propagation regime into either Sub- or Trans-sonic requires the determination of the shear wave speed. For linear elastic materials, shear wave speed is computed as $c_s = \sqrt{G/\rho}$, where G and ρ are the shear modulus and density, respectively. However, for elastomers, the computation is not straightforward because of the non-linear strain measures and material behavior. Corre et al. (2020) uses the expression developed in Boulanger and Hayes (2001) to compute c_s using the Mooney–Rivlin model. The computed shear wave speed under planar loading and the coefficients in Section 3.4 can be seen as a blue line in Fig. 1. The material density has been taken to be 1100 kg/m^3 Corre (2018).

As mentioned earlier, the specimen that is 40 mm tall has been tested in Corre et al. (2020) and Transonic cracks were observed. The shear wave speeds (c_s) and the observed crack speeds vs the applied stretch can be seen in Fig. 1. Different symbols indicate the results from two batches. Figure 6 of Corre et al. (2020) also contains the crack opening profiles for different crack speeds.

In this section, the velocity and strain fields will be examined for the presence of discontinuities that were mentioned earlier. Transonic cracks in elastomers in mode-I have been reported as well in Petersan et al. (2004), Chen et al. (2011), Mai et al. (2020). However, those studies do not report any discontinuities in strain or velocity fields. Chen et al. (2011), Marder (2006) state that the crack opening behind a crack moving in the Transonic regime has a wedge shape. However,

no mention of the weak discontinuities has been made there as well.

2.3 Velocity and strain profiles

The velocity fields from different experiments, $\lambda = 1.7$ and 3.5, can be seen in the Fig. 2 along with the yy component of deformation gradient. The crack speed at $\lambda = 1.7$ is about 15 m s^{-1}and at $\lambda = 3.5$ is about 56 m s^{-1}(Fig. 1). The shear wave speed, c_s, computed can be seen to be about 40 m s^{-1}. Hence, with respect to c_s, the former crack is subsonic and the latter is Transonic.

It can be seen from the Fig. 2a and c that the velocity magnitude fields do not show a significant difference in the form between the two experiments. The maximum value can, however, be seen to be higher in the case of stretch level of 3.5 as expected because of a higher crack speed. A similar comment can be made regarding the yy component of deformation gradient, although the values higher than 1 can be observed in the regions behind the tip for 3.5 case. However, a jump in any of these quantities has not been observed (compare with Figs. 13 and 14—details of which will be discussed later).

In addition to the above, the variation of velocity magnitude along a line about 5 mm above the crack path has been plotted in Fig. 3 for both 1.7 and 3.5 cases. There is a gradual increase in particle speeds as the crack tip is approached, maximum value observed behind the tip because of the crack faces moving apart as the tip passes through. The variation of yy component of the deformation gradient can be seen in the Fig. 4 for both the cases. Both fields can be seen to be continuous—there is no jump observed which wouldn't have been the case should there be a shock front present.

This article, hence, addresses the following questions—'Why don't we observe shocks in the bulk material even when a crack propagating in an elastomer travels faster than the shear wave (in the transonic regime)? Which material model more appropriately captures the behavior of the bulk material?'.

2.4 The residual strains

An additional observation has been made from the fracture tests on the 40 mm tall specimen. As mentioned earlier, a Pure Shear specimen is stretched to a required value and a seed crack is initiated using a razor blade on the left edge. The crack then runs from the left to the right edge. When the crack is just near the right edge (for example at about 20 mm from the right edge), it has been observed that the specimen at the left does not go back to zero strain level—some residual strain is left behind (Fig. 4), which eventually goes to zero after about a few minutes to few days after the experiment. The strain level at the left end at the instant described depends on the initial stretch and hence the crack speed. This indicates the presence of relaxation times that are larger than the duration of the experiment, that is typically about 10 ms. The yy-component of deformation gradient near the left edge are seen to vary between 1.1 and 1.9 for prestretch levels between 1.7 and 3.5.

Such observations have also been made during the retraction tests performed on the rubber, for example, in Niemczura and Ravi-Chandar (2011b), Mason (1963) and even during the experiments related to the propagation of cracks (Kadir and Thomas 1984). The cited references attribute this effect to the presence of relaxation times that are larger than the duration of experiment—in short, viscoelasticity. The other studies on dynamic cracks such as Petersan et al. (2004), Chen et al. (2011), Gent and Marteny (1982) do not report such an observation.

3 FE simulations

In this section, it will be examined, using the available experimental data, if the increase in modulus of the material because of an upturn in stress strain curve in uniaxial case is sufficient to capture the response of the bulk material for crack speeds in Transonic regime, using the methodology that will be explained below.

3.1 Simulation methodology

As mentioned in the earlier section, DIC technique has been used to obtain the displacement fields throughout the experiment. These fields are available everywhere in the body, except for some regions near the crack tip, crack faces and other boundaries. It is intended to check if the material model can reproduce the fields observed in the experiments if appropriate crack speed history and boundary conditions are imposed. For this purpose, the horizontal and vertical displacement val-

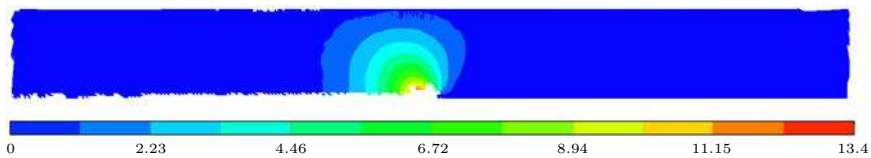

(a) Particle velocity magnitude ($\mathrm{m\,s^{-1}}$) for $\lambda_y = 1.7$.

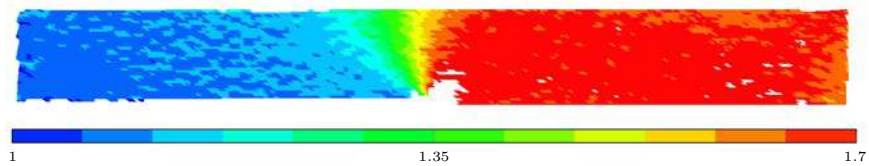

(b) Deformation gradient, F_{yy} for $\lambda_y = 1.7$.

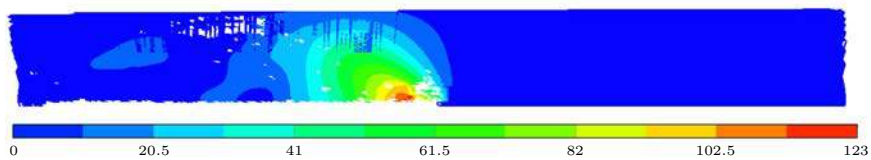

(c) Particle velocity magnitude ($\mathrm{m\,s^{-1}}$) for $\lambda_y = 3.5$.

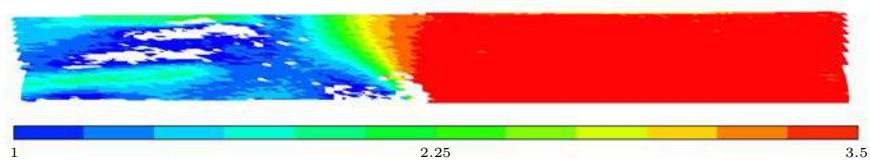

(d) Deformation gradient, F_{yy} for $\lambda_y = 3.5$.

Fig. 2 Experimental results plotted on undeformed configuration. **a** Particle velocity magnitude ($\mathrm{m\,s^{-1}}$) for $\lambda_y = 1.7$. **b** Deformation gradient, F_{yy} for $\lambda_y = 1.7$. **c** Particle velocity magnitude ($\mathrm{m\,s^{-1}}$) for $\lambda_y = 3.5$. **d** Deformation gradient, F_{yy} for $\lambda_y = 3.5$

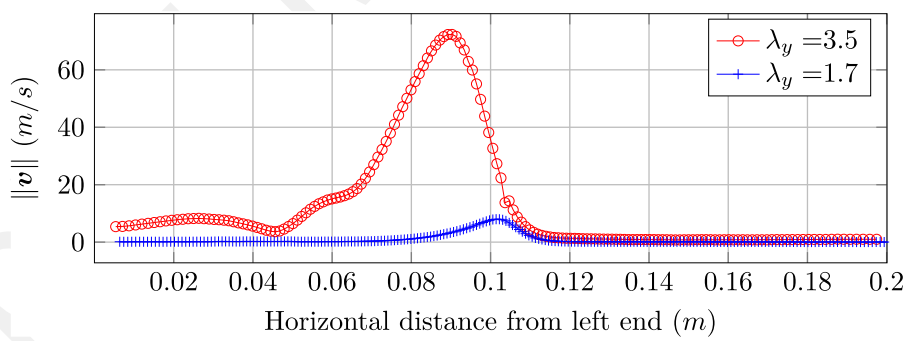

Fig. 3 Particle velocity distribution for two different stretches about 5 mm above the crack path

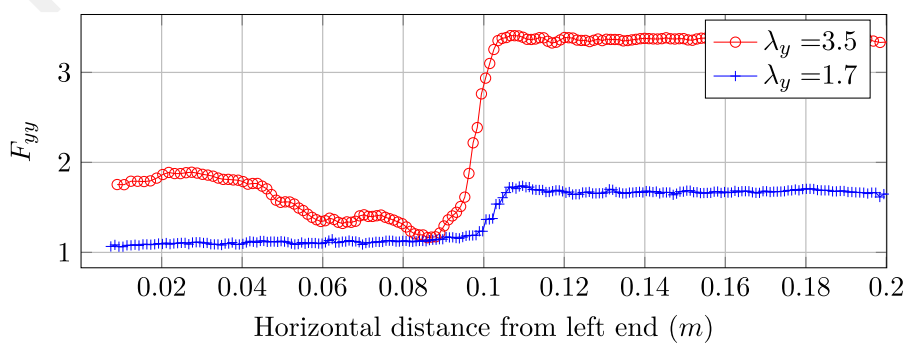

Fig. 4 Vertical component of deformation gradient, F_{yy}, distribution for two different stretches about 5 mm above the crack path

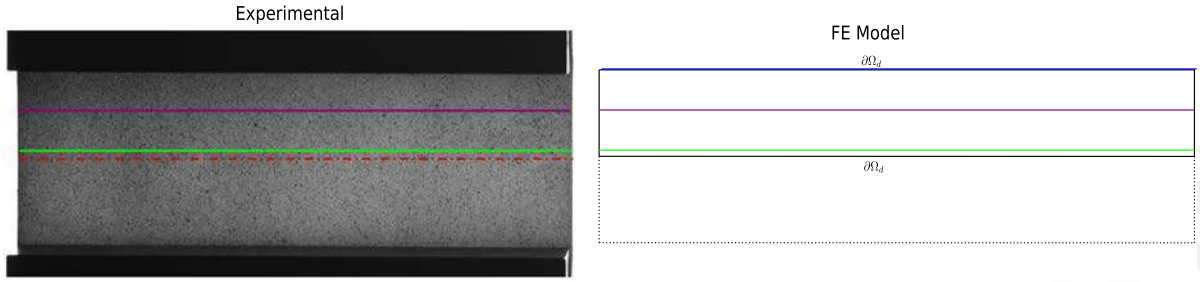

Fig. 5 Data extraction from experiments as input to FE model

Table 1 Model co-efficients

Parameter	C_{10}	C_{20}	C_{30}	C_{21}	C_{12}
Value (Pa)	1.044E6	−0.02273E6	336.0	124.0	−2.47

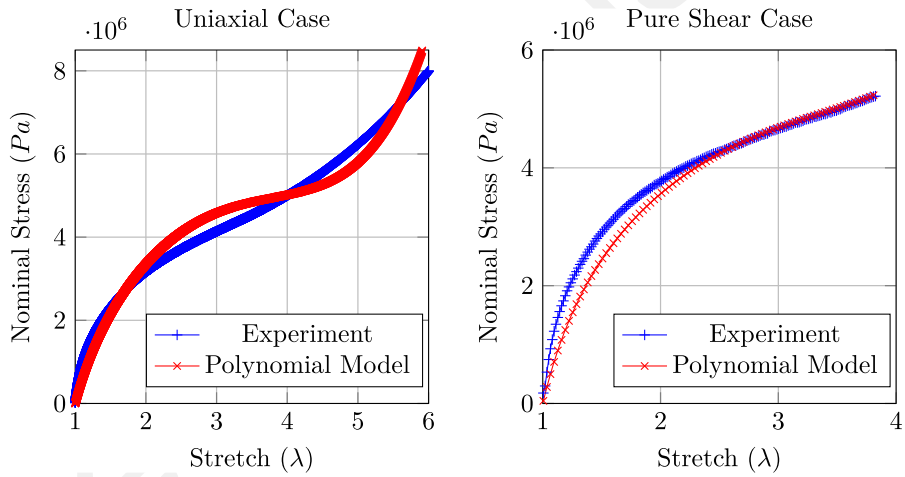

Fig. 6 Experimental results vs model prediction, uniaxial and pure shear case. Model coefficients in Table 1

ues are extracted along the green line as in the Fig. 5 all through the experiment. This data is then used as input for the simulations as boundary conditions (that change with time). The displacement and velocity profiles from the simulations are then compared to the experiments. The line along which the data are extracted (the green line) is about 1.5 mm away from the crack path (the red line).

It shall be noted that the crack propagation has not been explicitly modeled. Rather, the boundary conditions imposed are similar to when a crack passes through the material. The response of the bulk material under different constitutive assumptions will be examined and compared with the experiments. It is also possible to perform the current study by explicitly modeling the crack propagation by using a cohesive zone model, for instance. However, such an approach would require an additional assumption on the constitutive behavior of the failing material. As mentioned earlier, modeling of failing material be done in another article. The current approach bypasses that requirement by implicitly imposing the crack speed through boundary conditions.

The simulations have been performed using ABAQUS (Abaqus 2014) assuming that Plane Stress condition prevails (element CPS4 has been used). The HHT-α integration scheme (Hilber and Hughes 1976) has been used to evolve the solution in time. An element size of 0.3 mm has been used. The adaptive time step size is determined based on a half step residual criterion to ensure the accuracy of the solution.

3.2 Using a hyperelastic model

The Hyperelastic material model has been calibrated using the load-displacement data from uniaxial and pure shear tests. Additionally, a simulation has been performed on the Pure Shear case to check if the displacements predicted by the model match the displacements observed in the experiments. The results can be seen below. A polynomial model has been picked for the analysis as it has the ability to predict the upturn of the Stress–Strain curve—a phenomenon that is believed to promote Transonic cracks. The strain energy density for a polynomial model is (Rivlin and Saunders 1951)

$$W = \sum_{i+j=1}^{N} C_{ij}(\bar{I}_1 - 3)^i(\bar{I}_2 - 3)^j, \tag{1}$$

where $\bar{I}_1$ and $\bar{I}_2$ are the first and second invariants of the deviatoric part of Green strain tensor, $\bar{\boldsymbol{C}} = J^{-\frac{2}{3}}\boldsymbol{C}$ and J is the determinant of the deformation gradient. C_{ij}s are the model parameters. The resulting model co-efficients that are not zero can be seen in the Table 1.

It can be seen from the Fig. 6 that the model prediction does not exactly match the experimental load-displacement results for the uniaxial case. It was observed that moving the hyperelastic model closer to the uniaxial case reduces the capacity of the model to predict the deformed shape of the model under planar loading as can be seen in the Fig. 7. The black lines indicate the deformed shape observed in the experiments. Some modification in model parameters was needed to bring in the displacements closer to the experimental results. This lead to a slight difference in the model prediction in the uniaxial case. The model nonetheless exhibits an upturn in Stress strain response under uniaxial loading.

3.2.1 Results

In this section, results of simulations performed with just a hyperelastic material model will be discussed. The simulations have been carried out using the Polynomial model calibrated above. The simulation methodology will be discussed first, followed by the results and discussion.

(a) Model fitted to Uniaxial test only. Ogden model with $\mu_1 = 4.82\text{E-}2$ MPa, $\alpha_1 = 3.91$, $\mu_2 = 2.8$ MPa, $\alpha_2 = 0.27$ has been used (Corre, 2018).

(b) Current model parameters

Fig. 7 Deformed shape comparison, $\lambda_y = 3.5$. The black lines indicate the deformed shape from experiment. **a** Model fitted to Uniaxial test only. Ogden model with μ_1 = 4.82E−2 MPa, α_1 = 3.91, μ_2 = 2.8 MPa, α_2 = 0.27 has been used (Corre 2018). **b** Current model parameters

A half model has been used for the analysis, where the above extracted displacement fields are imposed on the bottom edge after initially stretching it to a target stretch level. It was observed that using $\alpha = 0$ for time integration did not result in convergence. Hence, a value of -0.33 has been used. Two cases have been analyzed - one for a stretch level of 1.7 and the other for 3.5. The results of the velocity and strain fields have been presented below and compared with the experimental results.

The velocity magnitude distribution from the FE simulation can be seen in the Fig. 8. It can clearly be seen that for a stretch level of 1.7, the results from the simulations match with that of the experiments (Fig. 2a) both qualitatively and quantitatively.

The velocity profile for the case of $\lambda = 3.5$ can be seen in the Fig. 9. In this case, it can be seen to be different from the experiments both quantitatively and qualitatively. As mentioned earlier, the crack speed in this case is 56 $\mathrm{m\,s^{-1}}$, which is greater than the shear wave speed, about 40 $\mathrm{m\,s^{-1}}$. It can be seen that the velocity magnitude increases sharply from 0 to about 120 $\mathrm{m\,s^{-1}}$in a span of two or three elements, that is

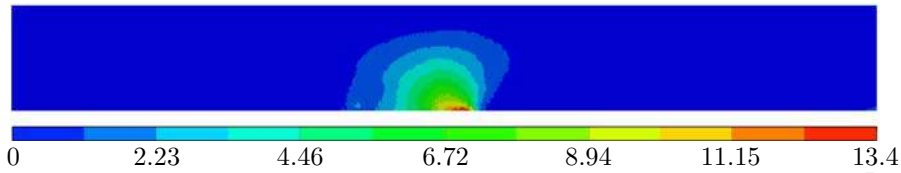

Fig. 8 Particle velocity magnitude using hyperelastic model (in m s^{-1}) for $\lambda_y = 1.7$ plotted on undeformed configuration

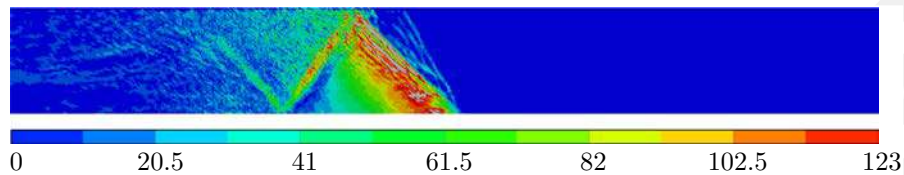

Fig. 9 Particle velocity magnitude using hyperelastic model (in m s^{-1}) for $\lambda_y = 3.5$ plotted on undeformed configuration

about 1 mm. The Fig. 10 shows the velocity variation along the length of specimen at about 5 mm above the crack path in FE simulations together with the results from the experiment. A clear difference can be seen between both the cases. In short, using a hyperelastic model can be seen to give a velocity profile that is close to the profile observed in the experiments for the subsonic case. The same, however, cannot be said about the transonic cracks even with a hyperelastic model with an upturn in uniaxial stress strain curve.

In the previously cited references Guo et al. (2003); Buehler et al. (2003), which considers an elastic material with such a stiffening behavior, a profile along which the fields exhibit jumps has been identified as seen in the FE simulations, but not in the experiments. Hence, at least for the current material, a Hyperelastic model may not be sufficient for the crack speeds enter the Transonic regime.

3.3 Inclusion of viscoelasticity

The previous section shows the inability of just a Hyperelastic model to reproduce the experimental results in Transonic regime. In this section, a viscoelastic model will be used with the Polynomial model described in the previous section for hyperelastic branch. The Finite Linear Viscoelatic model (Simo 1987) has been used for this purpose. It will be demonstrated that this model predicts the displacement and velocity fields to a good accuracy at least up to a stretch level of 3.5.

Stresses in the finite linear viscoelastic model can be expressed to be (Simo 1987)

$$\boldsymbol{S} = Jp\boldsymbol{C}^{-1} + J^{-\frac{2}{3}} DEV[\boldsymbol{H}], \tag{2}$$

where p is the pressure, $\boldsymbol{H}$ is the viscous over stress and DEV is the deviatoric projection in the reference configuration defined to be

$$DEV[\cdot] = \cdot - \frac{1}{3}(\cdot : \boldsymbol{C})\,\boldsymbol{C}^{-1}. \tag{3}$$

The viscous overstress is expressed as

$$\boldsymbol{H} = \int_{-\infty}^{t} g(t-s)\frac{\partial}{\partial s} DEV\left[2\frac{\partial \psi^0(\bar{\boldsymbol{C}})}{\partial \bar{\boldsymbol{C}}}\right], \tag{4}$$

where g is the memory kernel that can be expressed as $g(t) = g_\infty + \sum_{i=1}^{N} g_i e^{-\frac{t}{\tau_i}}$ in the case of linear viscoelasticity. Here, g_∞ and g_is indicate the ratio of the modulus of the hyperelastic and the viscous arms to the glassy modulus respectively. The model parameters g_i and τ_i can be found in Table 2. The time integration of the term $\boldsymbol{H}$ is performed using the technique presented in Taylor et al. (1970).

For the plane stress analysis, the value of p is found by using the condition that the out-of-plane stress component S_{33} is zero. The initial model parameters were initially obtained from DMA tests performed on the 40 mm specimen batch in Corre (2018). The polynomial model from the previous section has been chosen for the hyperelastic part. Adding viscoelasticity removes the shock-front-like feature that was observed in Fig. 9 and the velocity distribution looks qualitatively like that of the experiments. To match the results even quantitatively, the model coefficients have further been refined using the FE simulations based on the boundary conditions from crack experiments using the methodology of the previous section. A default value of -0.05 has been used for α in time integration.

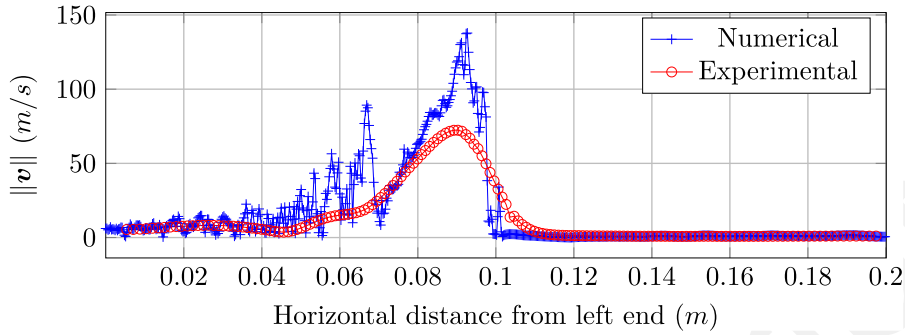

Fig. 10 Comparison of particle velocity magnitudes between experiments and simulations for Hyperelastic case, $\lambda = 3.5$ about 5 mm above the crack path

Table 2 Viscoelastic model parameters

Branch(i)	1	2	3	4	5	6	7	8	9	10
g_i	0.7312	0.02	0.02	0.2	0.01	0.005	0.0014	0.0011	0.0012	0.0005
τ_i(s)	1E−10	1E−9	1E−8	1E−7	1E−6	1E−5	1E−4	1E−3	1E−2	1E−1

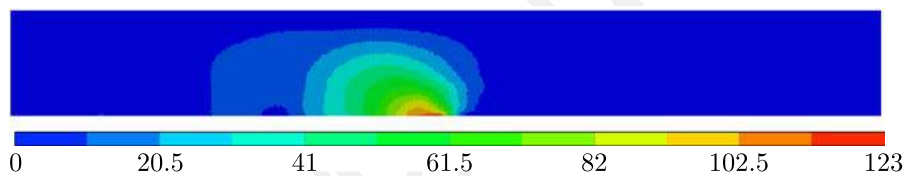

Fig. 11 Particle velocity magnitude using viscoelastic model (in m s^{-1}) for $\lambda_y = 3.5$ plotted on undeformed configuration

3.3.1 Results

If Viscoelastic model with the corrected model parameters is used to perform the FE simulations like in the previous section, the velocity profile looks like in the Fig. 11.

It can be seen from Fig. 11 (to be compared with Figs. 2c and 9) that the results from simulation with viscoelastic model are closer to the experimental results both qualitatively and quantitatively for Transonic case. The particle velocities from the experiments and the simulations plotted on the deformed configuration can be seen in the Fig. 12.

The variation of velocity magnitude along a length of the specimen at a distance of about 5 mm in the undeformed configuration can be seen in the Fig. 13 together with the experiments and Hyperelastic based FE simulation. The velocity distribution in the FE simulation with viscoelasticity can be seen to be quite close to the experimental results.

The yy-component of deformation gradient at about 5 mm above the crack path can be seen in the Fig. 14. A sharp 'jump' can be observed for the hyperelastic case, similar to what has been observed for the velocity variation. The viscoelastic case is closer to the experimental result. Also, the yy-component of the Cauchy stress tensor along the same path can be seen in the Fig. 15 for hyperelastic and viscoelastic cases. Consistent with the *jump* in the velocity magnitudes seen, a corresponding jump in the stress component can be seen in the hyperelastic case. A smooth and continuous variation for the viscous case can also be seen. Its variation along the data extraction line (1.5 mm above the crack path), behind the tip, can be seen in Fig. 16.

Appendix A contains further analysis where the position of data extraction line is changed to see if it impacts the results in any manner.

3.4 Viscoelastic model with Mooney–Rivlin hyperelastic branch

In the above presentation, the viscoelastic model has been used together with a hyperelastic model that exhibits an upturn in the stress strain response. In this subsection, the effect of using a hyperelastic model that does not exhibit this upturn in the stress-strain response in parallel with the Viscous branches will be examined. Mooney–Rivlin (MR) model has been chosen for this

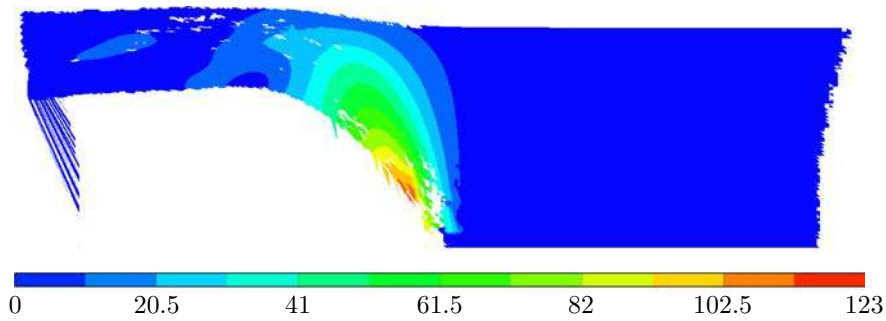

(a) Experimental result.

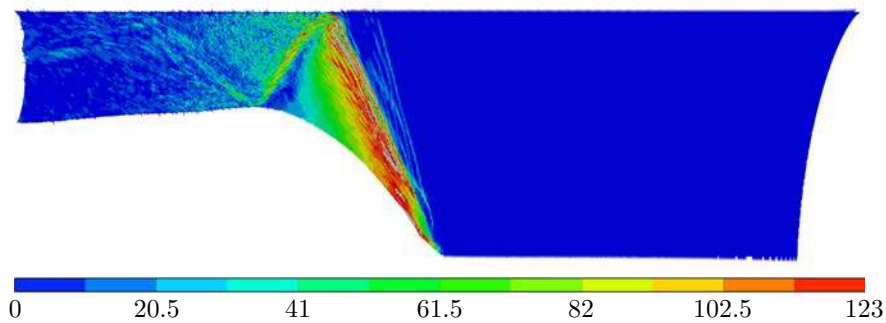

(b) Simulation with hyperelastic model.

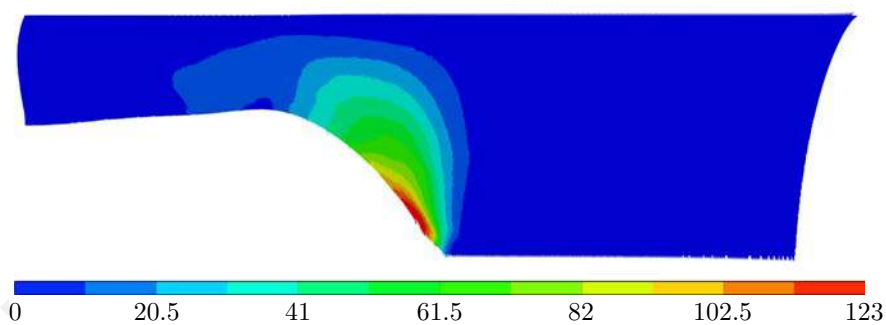

(c) Simulation with viscoelastic model.

Fig. 12 Particle velocity magnitude ($\mathrm{m\,s^{-1}}$) for $\lambda_y = 3.5$ plotted on deformed configuration. **a** Experimental result. **b** Simulation with hyperelastic model. **c** Simulation with viscoelastic model

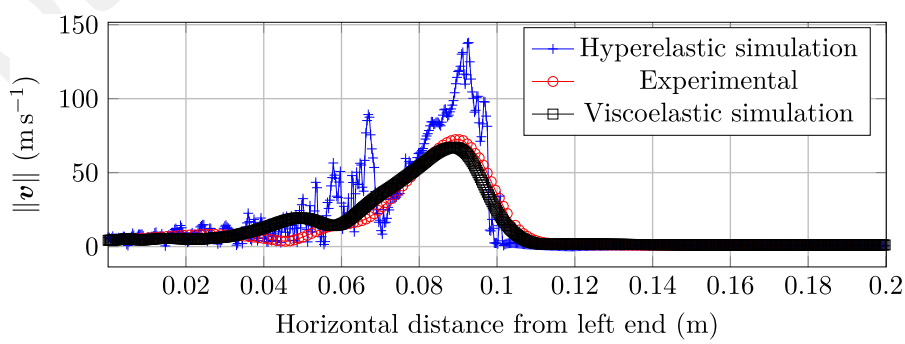

Fig. 13 Comparison of particle velocity magnitudes between experiments and simulations for Hyperelastic and viscoelastic cases, $\lambda = 3.5$ about 5 mm above the crack path

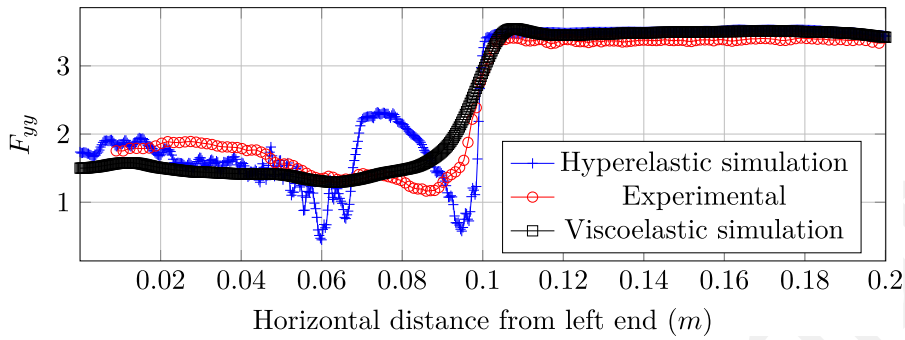

Fig. 14 F_{yy} comparison between simulations and the experiment for $\lambda_y = 3.5$, about 5 mm above the crack path

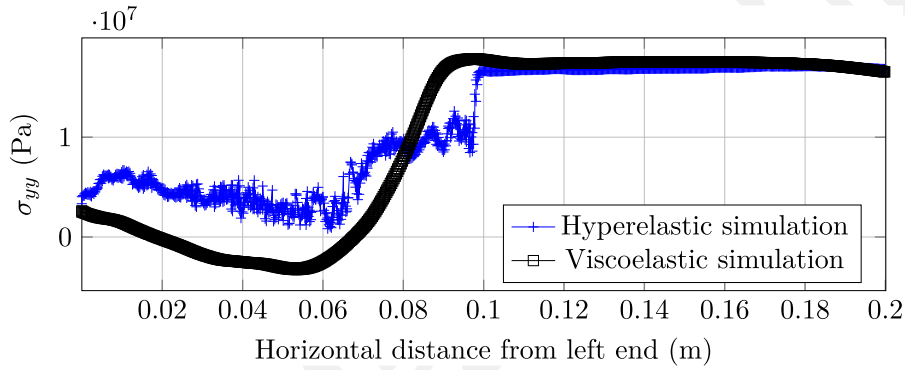

Fig. 15 yy-component of Cauchy stress about 5 mm above the crack path, $\lambda_y = 3.5$

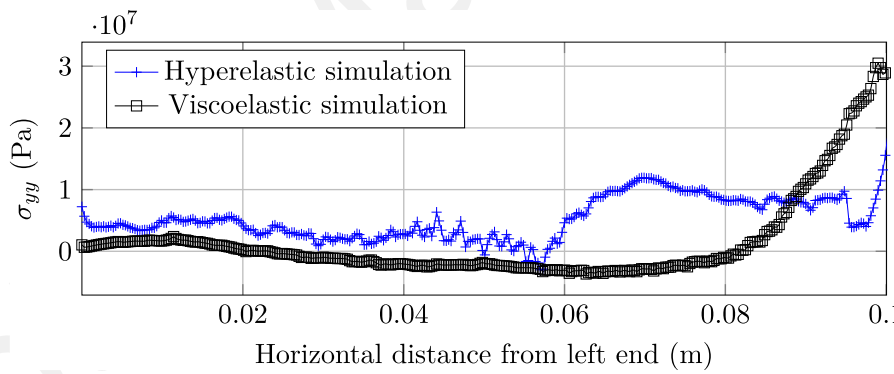

Fig. 16 yy-component of Cauchy stress behind the tip along the data extraction line (1.5 mm above the crack path), $\lambda_y = 3.5$

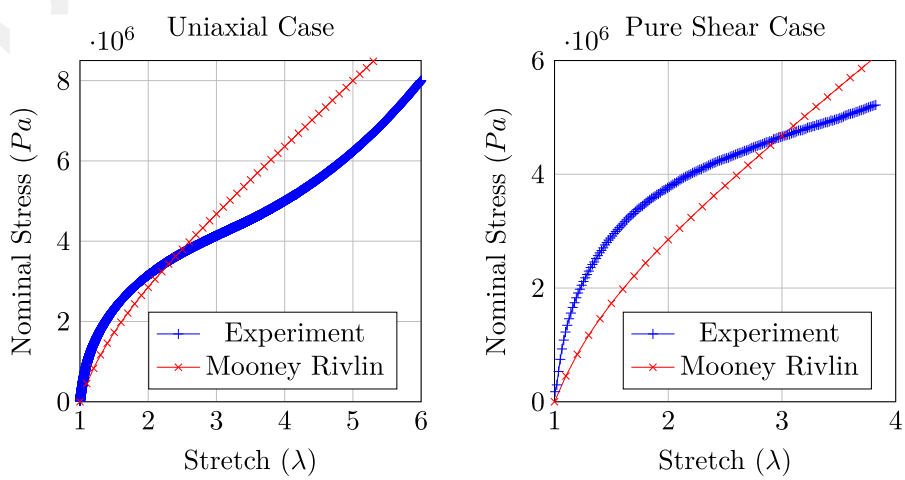

Fig. 17 Experimental results vs model prediction (Mooney–Rivlin), uniaxial and pure shear case

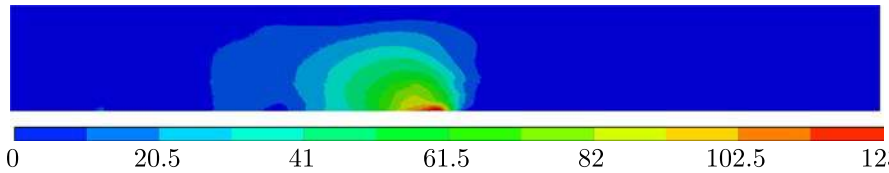

Fig. 18 Particle velocity magnitude (in m s^{-1}) with Mooney–Rivlin Hyperelastic branch plotted on undeformed configuration, $\lambda_y = 3.5$

Fig. 19 Comparison of results for particle velocities with Mooney–Rivlin and Polynomial Hyperelastic branches, $\lambda_y = 3.5$, about 5 mm above the crack path

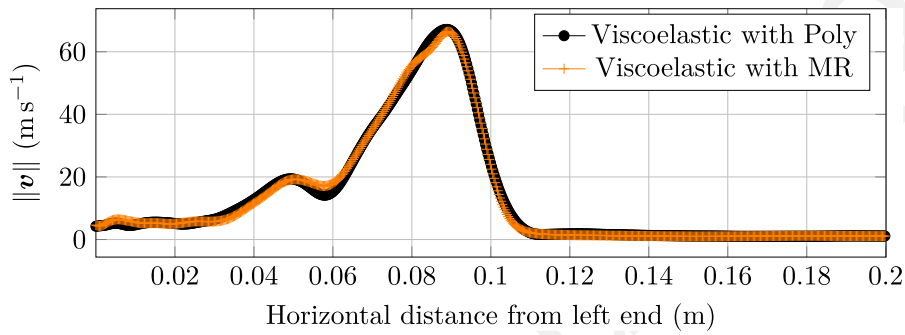

purpose. The strain energy function for this model is (Rivlin and Saunders 1951)

$$W = C_{10}(\bar{I}_1 - 3) + C_{01}(\bar{I}_2 - 3). \tag{5}$$

For the material at hand, $C_{10} = 0.8$MPa and $C_{10} = 0.03$MPa. The uniaxial and planar response of this model together with the experimental data can be seen in Fig. 17. Similar to the Polynomial model, the model response can be seen to differ from the experiments with the co-efficients chosen. This is to ensure that the displacement predictions by the model are closer to the experiments in pure shear case (similar to Fig. 7).

The simulation in the previous section for the Transonic case has been performed againwith theMooney–Rivlin hyperelastic branch. The resulting velocity profile can be seen in the Fig. 18 (to be compared with Figs. 2c and 11).

It is quite clear that the velocity distribution exhibits no 'jumps' even in this case. Also, the variation of velocity along the specimen about 5 mm above the crack path can be seen in the Fig. 19, along with the result from the previous section.

No significant difference can be seen between the two cases. Hence, the hyperelastic stiffening can be deemed to be neither necessary nor sufficient for the crack to enter the Transonic regime at least for the material at hand.

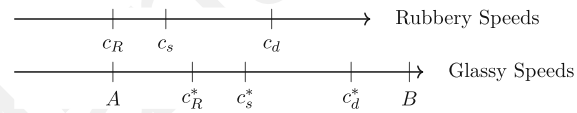

Fig. 20 Rubbery and glassy wave speeds in linear viscoelasticity. *R* Rayleigh, *s* shear, *d* dilataional. A and B indicate the possible range of the wave speeds that depend on the glassy to rubbery modulus ratio

4 Discussions

The previous sections contain the results from the experiments together with the results from FE simulations with hyperelastic and viscoelastic models. Experiments indicate that a 'shock front' was not observed even after the crack speeds exceed the elastic shear wave speed—a jump has not been observed either in velocity or strain fields which would have been the case if a shock front was present.

The crack speeds have been observed to exceed the shear wave speed in other studies in the literature like Petersan et al. (2004), Chen et al. (2011) and Mai et al. (2020). The material tested in Chen et al. (2011) is Latex rubber and the tests were performed at 85 °C to prevent strain crystallization. SBR was tested in Mai et al. (2020). The current study is performed on Polyurethane. The strain fields reported in Mai et al. (2020) do not exhibit any jumps as is the case in the current study even for crack speeds in Transonic regime. Chen et al. (2011) does not report any such shock fronts

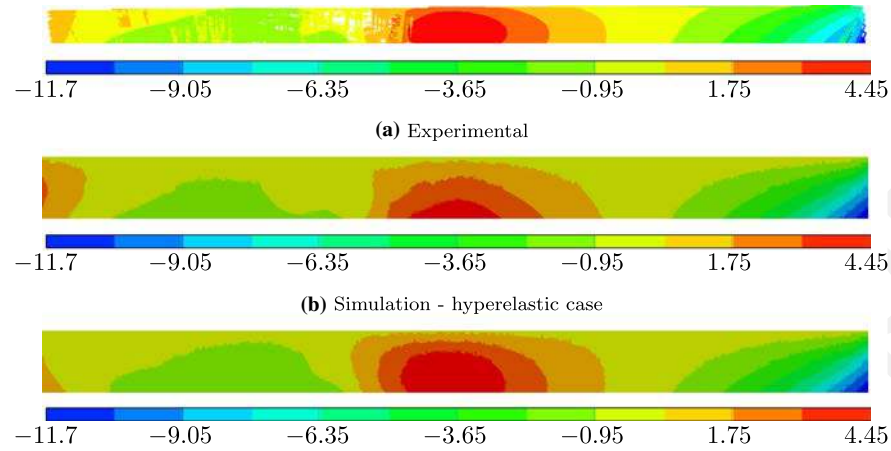

Fig. 21 Horizontal displacement (in mm) results for $\lambda_y = 3.5$ plotted on undeformed configuration. **a** Experimental, **b** Simulation—hyperelastic case, **c** Simulation—viscoelastic case

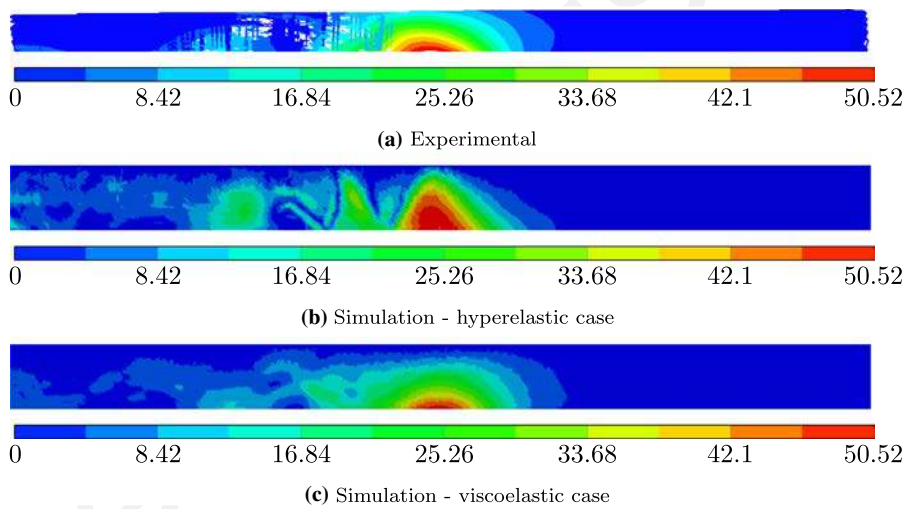

Fig. 22 Particle velocity magnitude (in m s^{-1}) results for $\lambda_y = 3.5$ plotted on undeformed configuration. **a** Experimental. **b** Simulation—hyperelastic case. **c** Simulation—viscoelastic case

as well, but instead report that the crack faces in this regime are wedge shaped (which were noted to resemble a shock front in Petersan et al. (2004)).

An interesting comparison can be made regarding the ratios of crack speed to the shear wave speed at a prestretch level of 3.5 in different studies. In Mai et al. (2020), the speed ratio can be seen to be 1.84, while in Chen et al. (2011), the ratio is smaller than 1.25. In the current study, the ratio is about 1.38. This indicates perhaps an obvious conclusion that the material properties (mainly viscoelasticity) determine the extent to which the crack speed can exceed the shear wave speed.

The hyperelastic model calibrated using the uniaxial and pure shear cases is used to perform FE simulations with the displacements extracted from the experiments in Corre et al. (2020). It shall be noted that the hyperelastic model does not exactly follow the Uniaxial stress–strain curve. The calibrated model, however, is seen to exhibit an upturn in the stress–strain curve which is usually deemed to be one of the reasons for crack speeds to go into Transonic regime (Gent and Marteny 1982; Stevenson and Thomas 1979; Buehler et al. 2003). The FE result using this model, however, is seen to produce 'jumps' in both the velocity and strain fields for the cases when the crack speeds are Transonic—a result not seen in the experiments.

Including viscoelasticity is seen to bring the results closer to the experiments. The strain and velocity fields no longer exhibit the discontinuities that were observed in the hyperelastic case. The maximum horizontal displacements and the velocity magnitudes have been observed to be within 10 % of the experiment results.

The crack faces behind the tip, being a free edge, is ideally traction-free. As presented in Fig. 4, the residual strains behind the tip are non-zero. The computation of tractions from strains involves making a constitutive assumption about the material. Using a hyperelastic model in the simulations results in non-zero stresses along the edge as a consequence of the non-zero strain (despite it being a free edge in the experiments). See Fig. 16, where the yy component of Cauchy stress is plotted along the data extraction location (1.5 mm above the crack path). However, using a viscoelastic model with relaxation times that are comparable to the duration of the experiment, the stresses along the edge behind the tip quickly drop to small values within 15 % of the far-field stresses (and smaller than in the hyperelastic case). Refining the model further can perhaps bring even those stresses to zero.

Hence, at least for the material in the current study, the cracks can go Transonic as a result of the viscoelastic 'stiffening' of the material. A suggestion of this kind can be found in Stevenson and Thomas (1979). However, no evidence has been presented in that study as to whether the Transonic cracks are a result of Viscoelastic stiffening or hyperelastic stiffening. A similar comment has been made in Marder (2006). However, in that work, a Kelvin type model has been assumed for the elastomer where the wave speeds increase unboundedly with the frequency. Hyperelastic stiffening has been deemed to be not necessary, but its sufficiency has not been discussed. In studies where this sufficiency has been studied Buehler et al. (2003), 'Mach cones' corresponding to shear waves were reported that tail the crack tip (Figure 4 of the reference).

The notion of limiting speed for a crack comes from the inclusion of inertial effects in the study of the problem (Freund 1990). The LEFM establishes the limiting speed as the Rayleigh wave speed in mode-I, while in mode-III, it is the Shear wave speed based on the elastic properties of the material. In studies where the inertial effects are included together with Viscous effects (Graham and Walton 1995; Atkinson and Popelar 1979; Willis 1967), the limiting speed is seen to depend on the *glassy* modulus of the material rather than on the *rubbery* modulus (Fig. 20). Hence, the crack is allowed to exceed the rubbery shear wave speed. Such a result can also be observed in Geubelle et al. (1998), where spectral methods are used to investigate the problem of viscoelastodynamic mode-III crack. Using a rate independent cohesive zone type model, an analysis has been made on the effect of relaxation times on crack speeds. From Figure 11 of the reference, it can clearly be seen that the crack speed exceeds the *rubbery* shear wave speed (c_s), but remains smaller than the *glassy* shear wave speed (c_s^*). However, no specific comments have been made in regards to the presence or absence of shock fronts in those references.

In Fisher and Gurtin (1965), the propagation of waves of order N in viscoelastic media has been studied. Waves of order N have the solution, $\boldsymbol{u}$, which is $N-1$ times continuously differentiable and exhibit discontinuities in the Nth derivative along a hypersurface. It has been determined in that study that such waves, should they exist, travel with a speed that is derived based on the glassy modulus of the material rather than the rubbery modulus. Shock fronts, by definition, are waves of order 1 and hence travel with that speed as well. Hence, it might be possible that shock fronts can be observed in viscoelastic material only when the crack speed exceeds even the glassy shear wave speed of the material. In short, a weak discontinuity, should it exist, would be made of high frequency waves at the sharp front. As a consequence of viscoelasticity, this region behaves with a high modulus which in turn roughly raises the shear wave speeds to a value that is (equal to or) greater than the crack speed. This, in turn, prevents a shock wave from developing.

Perhaps, the cracks whose speeds exceed c_s while still remaining below c_s^* should be called r—Transonic (r stands for *rubbery*) to distinguish them from cracks that travel faster than c_s^*. One such instance may be found in Gori et al. (2018), where a mode-II crack propagating in a PMMA specimen along a weak plane has been studied experimentally. It was observed that because of the viscoelastic behavior of the material, the crack speed exceeds c_s^* (hence c_s) and c_d as well. Based on the inclination of the 'mach fronts' observed, the shear wave speed was computed and was seen to be in good agreement with the shear wave speed computed based on the modulus corresponding to the strain rates in that region.

5 Conclusions

This article revisits the experiments performed on Polyurethane elastomer in Corre et al. (2020) to study the phenomenon of Transonic cracks. The crack propagation has not been explicitly modeled. Instead, the dis-

placement fields extracted from the experiments using the DIC technique are used as input to perform FE simulations. This way, the crack speed is used as an input. The simulations have been performed first using a hyperelastic model with an upturn in the stress-strain curve. In the Subsonic case, particle velocities were seen to be closer to the experiments while in the Transonic case, a 'jump' was observed. Inclusion of viscoelasticity was seen to eliminate the 'jump' observed earlier and bring the results closer to the experiments. Inclusion of viscoelasticity results in the notions of 'rubbery' and 'glassy' wave speeds as opposed to the quasi-static hyperelastic case where only the 'rubbery' wave speed exists. More analyses have been performed with the viscoelastic model with the hyperelastic branch that does not exhibit the aforementioned upturn. The results were still observed to be closer to the experiments in the Transonic case. Hence, for the material in the current study, Transonic cracks are seen to be the consequence of 'viscoelastic stiffening' of the bulk material. Hyperelastic stiffening was seen to be not necessary.

Acknowledgements VK thanks Thomas Corre, Erwan Verron and Julien Réthoré for various discussions held on this subject.

Declarations

Conflict of interest The authors declare that they have no conflict of interest.

Appendix A: FE simulations for a different data extraction location

For the results of FE simulations presented in earlier sections, the boundary conditions were extracted along a line just above the crack path (green line in Fig. 5). To examine the effect of the location of data extraction line on the observed results, some more analyses have been performed where the data is extracted from the middle of the top half of the specimen instead of just above the crack path (purple line in Fig. 5). The new data extraction location is about 10 mm from the crack path in the undeformed configuration.

The analyses in the previous sections are then repeated with new data as boundary conditions. The results can be seen in Figs. 21 and 22.

Even in this case, the results of FE simulations with viscoelastic model can be seen to be closer to the experiments. In the case of horizontal displacements from Fig. 21, a bean shaped profile can be seen in the experimental result and the FE simulation with viscoelasticity. The case with just hyperelastic model does not exhibit this distinct profile. It shall be noted that the experimental result does not include the data near the top edge of the specimen.

Similarly, the velocity magnitudes from experiment and viscoelastic FE simulation are closer while hyperelastic result is not. This demonstrates the robustness of the viscoelastic model used and also indicates the presence of viscoelastic effects in regions far from the crack tip.

References

Abaqus UM (2014) Abaqus theory guide. Version 6(14)

Atkinson C, Popelar C (1979) Antiplane dynamic crack propagation in a viscoelastic strip. J Mech Phys Solids 27(5–6):431–439. https://doi.org/10.1016/0022-5096(79)90024-3

Boulanger P, Hayes M (2001) Finite-amplitude waves in Mooney–Rivlin and Hadamard materials, January 2001. https://doi.org/10.1007/978-3-7091-2582-3

Buehler MJ, Abraham FF, Gao H (2003) Hyperelasticity governs dynamic fracture at a critical length scale. Nature 426(6963):141–146. https://doi.org/10.1038/nature02096

Chen CH, Zhang HP, Niemczura J, Ravi-Chandar K, Marder M (2011) Scaling of crack propagation in rubber sheets. EPl. https://doi.org/10.1209/0295-5075/96/36009

Coret M, Corre T (2017) Investigation of dynamic fracture of elastomers—I. https://doi.org/10.5281/zenodo.4034638

Corre T (2018) Rupture dynamique de membranes élastomères : étude expérimentale par mesure de champs. PhD thesis

Corre T, Coret M, Verron E, Leblé B, Le Lay F (2020) Experimental full field analysis for dynamic fracture of elastomer membranes. Int J Fract 224(1):83–100. https://doi.org/10.1007/s10704-020-00447-1

Fisher GMC, Gurtin ME (1965) Wave propagation in the linear theory of viscoelasticity. Q Appl Math 23(3):257–263. https://doi.org/10.1090/qam/191196

Freund L (1979) The mechanics of dynamic shear crack propagation. J Geophys Res 84(B5):2199. https://doi.org/10.1029/JB084iB05p02199

Freund L (1990) Dynamic fracture mechanics. Cambridge University Press, Cambridge. https://doi.org/10.1017/CBO9780511546761

Gent AN, Marteny P (1982) Crack velocities in natural rubber. J Mater Sci 17(10):2955–2960. https://doi.org/10.1007/BF00644675

Geubelle PH, Danyluk MJ, Hilton HH (1998) Dynamic mode III fracture in viscoelastic media. Int J Solids Struct 35(9–10):761–782. https://doi.org/10.1016/S0020-7683(97)00084-X

Gori M, Rubino V, Rosakis AJ, Lapusta N (2018) Pressure shock fronts formed by ultra-fast shear cracks in viscoelastic materials. Nat Commun 9(1):4754. https://doi.org/10.1038/s41467-018-07139-4

Graham GAC, Walton JR (1995) Crack and contact problems for viscoelastic bodies

Guo G, Yang W, Huang Y (2003) Supersonic crack growth in a solid of upturn stress-strain relation under anti-plane shear. J Mech Phys Solids 51(11–12):1971–1985. https://doi.org/10.1016/j.jmps.2003.09.028

Hilber HM, Hughes TJR (1976) Taylor RL (1977) Improved Numerical Dissipation For Time Integration Algorithms in Structural Dynamics. Earthquake Eng Struct Dynam 5:283–292

Huang Y, Gao H (2001) Intersonic crack propagation-part I: the fundamental solution. J Appl Mech 68(2):169. https://doi.org/10.1115/1.1357871

Knowles James K (2002) Impact-induced tensile waves in a rubberlike material. SIAM J Appl Math 62(4):1153–1175. https://doi.org/10.1137/S0036139901388234

Kadir A, Thomas AG (1984) Tearing of Unvulcanized natural rubber. J Polymer Sci A 2 Polymer Phys 22(9):1623–1634

Mai TT, Okuno K, Tsunoda K, Urayama K (2020) Crack-tip strain field in supershear crack of elastomers. ACS Macro Lett 9(5):762–768. https://doi.org/10.1021/acsmacrolett.0c00213

Marder M (2006) Supersonic rupture of rubber. J Mech Phys Solids 54(3):491–532. https://doi.org/10.1016/j.jmps.2005.10.002

Mason P (1963) Finite elastic wave propagation in rubber. Proc R Soc A 272(1350):315–330. https://doi.org/10.1098/rspa.1963.0056

Morishita Y, Tsunoda K, Urayama K (2016) Velocity transition in the crack growth dynamics of filled elastomers: contributions of nonlinear viscoelasticity. Phys Rev E. https://doi.org/10.1103/PhysRevE.93.043001

Needleman A (1999) An Analysis of Intersonic Crack Growth Under Shear Loading. J Appl Mech 66(4):847. https://doi.org/10.1115/1.2791788

Niemczura J, Ravi-Chandar K (2011a) On the response of rubbers at high strain rates-I. Simple waves. J Mech Phys Solids 59(2):423–441. https://doi.org/10.1016/j.jmps.2010.09.006

Niemczura J, Ravi-Chandar K (2011b) On the response of rubbers at high strain rates-III. Effect of hysteresis. J Mech Phys Solids 59(2):457–472. https://doi.org/10.1016/j.jmps.2010.09.009

Petersan PJ, Deegan RD, Marder M, Swinney HL (2004) Cracks in rubber under tension exceed the shear wave speed. Phys Rev Lett 93(1):015504-1. https://doi.org/10.1103/PhysRevLett.93.015504

Ravi-Chandar K, Knauss W (1984) An experimental investigation into dynamic fracture: I. Crack initiation and arrest. Int J Fract 25(4):247–262. https://doi.org/10.1007/BF00963460

Rivlin RS, Saunders DW (1951) Large elastic deformations of isotropic materials VII. Experiments on the deformation of rubber. Philosoph Trans R Soc Lond Ser A 243(865):251–288

Rosakis AJ (2002) Intersonic shear cracks and fault ruptures. Adv Phys 51(4):1189–1257. https://doi.org/10.1080/00018730210122328

Rosakis AJ, Samudrala O, Coker D (2000) Intersonic shear crack growth along weak planes. Mater Res Innov 3(4):236–243. https://doi.org/10.1007/s100190050009

Sharon E, Gross SP, Fineberg J (1996) Energy dissipation in dynamic fracture. Phys Rev Lett 76(12):2117–2120. https://doi.org/10.1103/PhysRevLett.76.2117

Simo JC (1987) On a fully three-dimensional finite-strain viscoelastic damage model: formulation and computational aspects. Comput Methods Appl Mech Eng 60(2):153–173. https://doi.org/10.1016/0045-7825(87)90107-1

Stevenson A, Thomas AG (1979) On the bursting of a balloon. J Phys D Appl Phys 12(12):2101–2109. https://doi.org/10.1088/0022-3727/12/12/012

Taylor RL, Pister KS, Goudreau GL (1970) Thermomechanical analysis of viscoelastic solids. Int J Numer Methods Eng 2:45–59

VIC-2D CS (2009) Software; correlated solutions. https://www.correlatedsolutions.com/vic-2d/

Washabaugh PD, Knauss W (1994) A reconciliation of dynamic crack velocity and Rayleigh wave speed in isotropic brittle solids. Int J Fract 65(2):97–114. https://doi.org/10.1007/BF00032282

Willis J (1967) Crack propagation in viscoelastic media. J Mech Phys Solids 15(4):229–240. https://doi.org/10.1016/0022-5096(67)90013-0